Research Article

Influence of Fe Buffer Layer on Co-Doped BaFe$_2$As$_2$ Superconducting Thin Films

C. Bonavolontà,[1,2] C. de Lisio,[1,2] M. Valentino,[2] F. Laviano,[3] G. P. Pepe,[1,2] F. Kurth,[4] K. Iida,[4,5] A. Ichinose,[6] and I. Tsukada[6]

[1]*Dipartimento di Fisica, Università di Napoli Federico II, Via Cintia, Complesso di Monte S. Angelo, 80125 Napoli, Italy*
[2]*CNR-SPIN, Via Cintia, Complesso di Monte S. Angelo, 80125 Napoli, Italy*
[3]*Department of Applied Science and Technology, Politecnico di Torino, Corso Duca degli Abruzzi 24, 10129 Torino, Italy*
[4]*Institute for Metallic Materials, IFW Dresden, 01171 Dresden, Germany*
[5]*Department of Crystalline Materials Science, Nagoya University, Chikusa-ku, Nagoya 464-8603, Japan*
[6]*Central Research Institute of Electric Power Industry, 2-6-1 Nagasaka, Yokosuka 240-0195, Japan*

Correspondence should be addressed to C. Bonavolontà; bonavolo@na.infn.it

A systematic characterization of Co-doped BaFe$_2$As$_2$ (Ba-122) thin films has been carried out. Two samples were available, one grown on CaF$_2$ substrate and the other on MgO with an Fe buffer layer. The goal was to investigate films' magnetic and superconducting properties, their reciprocal interplay, and the role played by the Fe buffer layer in modifying them. Morphological characterization and Energy Dispersive X-ray analyses on the Fe-buffered sample demonstrate the presence of diffused Fe close to the Co-doped Ba-122 outer surface as well as irregular holes in the overlying superconducting film. These results account for hysteresis loops obtained with magneto-optic Kerr effect measurements and observed at both room and low temperatures. The magnetic pattern was visualized by magneto-optical imaging with an indicator film. Moreover, we investigated the onset of superconductivity through a measure of the superconducting energy gap. The latter is strictly related to the decay time of the excitation produced by an ultrashort laser pulse and has been determined in a pump-probe transient reflectivity experiment. A comparison of results relative to Co-doped Ba-122 thin films with and without Fe buffer layer is finally reported.

1. Introduction

Recently, tremendous efforts have been made to obtain reliable information on fundamental properties of iron-based superconductors (IBS), such as superconducting energy gaps, nature of excitation assisting Cooper pair formation, and (ferro)magnetism. On the other hand, many applications based on Josephson effect have been proposed and realized, for example, Superconducting Quantum Interference Devices (SQUIDs) [1] and Single Flux Quantum (SFQ) devices.

Thin films are often preferred for applications in superconducting electronics, and, due to their controlled geometries, also for studying both transport and optical properties. Within the family of IBS, Co-doped BaFe$_2$As$_2$ (Ba-122) thin films are among the most promising candidates for superconducting applications due their relatively easy fabrication through pulsed laser deposition [2–4].

In this work, we investigate magnetic and superconducting properties of Co-doped Ba-122 thin films with and without Fe buffer layer. We focussed our attention on the effect of an Fe buffer layer deposited on MgO (001) substrate by comparing the thin film behaviour with that of a similar film deposited on CaF$_2$ substrate (without Fe layer). The Fe buffer layer acts as a strain absorber, leading to both sharp out-of-plane and in-plane texture [5–7]. However, its role is not yet completely clear. For example, it is not known how ferromagnetism due to the Fe buffer layer influences spin density waves (SDWs) and superconducting states of Ba-122. Optical techniques are very effective in isolating

the contributions of different films to the overall sample properties: As an example, tuning the wavelength of incident radiation implies different penetration depths, thus allowing probing inner layers inside the material.

In particular, time-resolved spectroscopy is a suitable technique to study electronic excitations in superconductors, like IBS [8–10], since in the low-excitation regime different coexisting excitation/relaxation processes can be identified by their specific lifetimes [11, 12]. In IBS, ultrafast spectroscopy has been used to reveal the existence of pseudogap states [8], competition between SDWs and superconducting states [13] and to understand the role of interband interactions and gap symmetry [14]. Moreover, this technique ultrafast spectroscopy has been used to investigate quasiparticle (QP) dynamics in Ba-122 family, proving its ability to reveal the multigap nature of such superconductors [15].

We also report on additional characterization of Co-doped Ba-122 samples with magneto-optical imaging (MOI) and magneto-optical Kerr effect (MOKE). The magneto-optical Kerr effect (MOKE) technique reveals sample magnetization as a function of external magnetic field. It represents a powerful method to determine local magnetic properties of thin films [16]. In fact, unlike conventional techniques, such as vibrating sample magnetometer (VSM) and SQUID susceptometer [17], providing information on the average magnetization of the whole sample volume, this technique is simply implemented and capable of probing the sample magnetization with a spatial resolution limited by the laser beam spot size.

In addition, Atomic Force Microscopy (AFM), Transmission Electron Microscopy (TEM), and Energy Dispersive X-ray (EDX) analyses allowed us to determine both morphology and local analytical composition of Co-doped Ba-122 thin films, which is of particular interest in presence of the iron buffer layer.

Finally, by means of different optical techniques, namely, MOKE, MOI, and ultrafast spectroscopy, we could establish the role of Fe buffer layers on magnetic and superconducting properties of our Ba-122 samples.

2. Materials and Experimental Set-Up

In this work, we have studied two films, namely, $Ba(Fe_{1-x}Co_x)_2As_2$ on Fe-buffered MgO substrate and $Ba(Fe_{1-x}Co_x)_2As_2$ on bare CaF_2. From now on, these two samples shall be referred to as Ba-122/Fe and Ba-122. The estimated Co content in both samples was $x = 0.08$ (optimal doping).

The Ba-122/Fe bilayer was prepared by pulsed laser deposition (PLD) on MgO substrate using a polycrystalline target with high phase purity. Ba-122 and Fe films were 100 nm and 20 nm thick, respectively. We then deposited 100 nm thick Ba-122 film on (001) CaF_2 substrate.

In situ reflection high energy electron diffraction (RHEED) confirmed that both Fe and Co-doped Ba-122 films were epitaxially grown. Moreover, X-ray diffraction proves single phase formation of Co-doped Ba-122, whereas pole figure measurements further verify the epitaxial growth of Fe and Co-doped Ba-122 with the following relation:
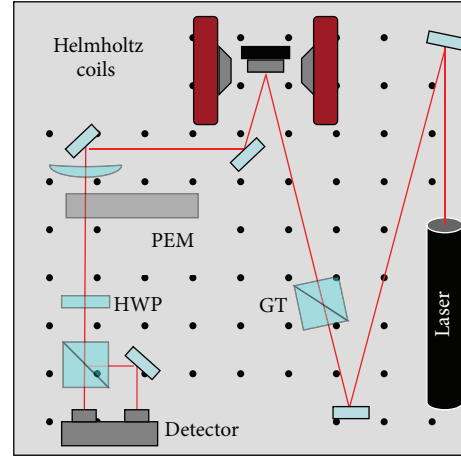

FIGURE 1: MOKE set-up: GT: Glan-Thompson polarizer; HWP: half-wave plate; PEM: photoelastic modulator.

(001)[100]Ba-122∥(001)[110]Fe∥(001)[100]MgO. More details about sample preparation can be found in [5–7].

Typically, growing epitaxial Co-doped Ba-122 thin films on bare MgO substrate leads to low quality superconducting films. As reported in [18], this is presumably due to the weak epitaxial strain connected to the film grain orientation, depending in turn on the thermal expansion coefficient of the substrates. However, we found that CaF_2 proved to fulfil many requirements for growing epitaxial Ba-122 of good quality and without any buffer layer [5, 6]. On the other hand, mixing also occurs at Fe/CaF_2 interface, giving rise to imperfect compounds [19]. Consequently, the comparison of Ba-122 film with Ba-122/Fe bilayer must necessarily be performed with different substrates. It has been demonstrated that these two samples showed almost the same crystalline quality and superconducting properties [5–7].

The superconducting transition temperatures of the Ba-122 and Ba-122/Fe thin films were measured by a 4-probe method and turned out to be 25.4 K and 26.3 K, respectively.

Using AFM and TEM analyses, both morphological properties and transverse sections of the bilayer have been investigated. TEM imaging supported by EDX analysis evidenced the different distribution of Ba, Fe, and As into the sample.

In order to investigate local magnetic properties of the samples, we recorded hysteresis loops based on longitudinal MOKE. The experimental set-up is reported in Figure 1. The He-Ne laser beam lies in the horizontal plane and its radiation is linearly polarized in the vertical direction by a Glan-Thompson (GT) polarizer with an extinction ratio of 10^{-6}. Due to geometrical constraints determined by the Helmholtz coils, the angle of incidence is about $20°$. A 300 mm focal length lens focuses the light beam onto the sample surface. The reflected beam is modulated at 50 kHz frequency by a photoelastic modulator (PEM) (Hinds Instruments, mod. PEM-90). The modulated beam is then transmitted through a half-wave plate- (HWP-) polarizing beam-splitter (PBS) system and is finally detected by a fast responding diode-bridge detector (New Focus, mod. Nirvana 2007). The latter

generates the input signal to a lock-in amplifier (EG&G, mod. 7260) whose reference signal is provided by the PEM driver electronics. A pair of Helmholtz coils powered by a bipolar power supply (Elind, mod. KL 1200) generates the external magnetic field up to 1 T. The magnetic field intensity is measured with a Hall sensor (Leybold, mod. 516-60) placed within the electromagnet gap, close to the sample surface. To perform low temperature measurements, the sample is placed on a cold finger inside a temperature controlled, liquid helium, continuous flow, optical cryostat operating down to 5 K.

Moreover, magnetic images of the samples were obtained by means of MOI technique, performed with an optical microscope equipped with polarization optics and a garnet indicator film [20]. In MOI pictures the light contrast is proportional to the out-of-plane magnetic field component (the brighter the contrast appears, the larger the normal component of the magnetic field is). The local magnetic moment of the sample is visualized in real-time, with microscopic resolution on the whole sample surface. Details of the technique are reported in [20]. The MOI technique achieves identification of the magnetic response in the temperature range 4 K–300 K with an applied magnetic field up to 0.2 T. In MOI pictures the light contrast is proportional to the out-of-plane magnetic field component (the brighter the contrast appears, the more intense the magnetic field pointing toward the reader is).

Additionally, time-resolved reflectivity measurements were performed using a standard pump-probe technique, based on a mode-locked Ti:Sa laser, delivering pulses at 82 MHz repetition rate, 100 fs duration, 800 mW average power, and 795 nm center wavelength. The sample was mounted in the same cryostat used for MOKE measurements. Further details on the experimental methods can be found in [21]. The photoinduced normalized reflectivity change $\Delta R/R$, as a function of time, was measured using a pump fluence of $12\,\mu$J/cm^2 and 20 times weaker probe.

3. Results and Discussion

TEM analysis and AFM characterization of the Ba-122/Fe bilayer are reported in Figure 2. The AFM image (Figure 2(a)) shows some holes on the sample surface, indicating that the surface is not flat. This result is confirmed by the TEM image (Figure 2(b)), where the presence of holes on the superconductor surface is quite evident.

Moreover, the Ba-122 (100 nm)/Fe surface also presents considerable degradation, most likely due to direct exposure of the samples to the atmosphere. This effect has already been reported in literature [22], where an inhomogeneous and partially degraded surface layer in Fe-based pnictides was observed.

As reported in [23] the AFM measurement on Ba-122 sample on CaF$_2$ substrate shows a typical multilayered surface with some smooth terraces.

An estimate of the holes dimensions (see Figure 2(b)) has been carried out. Their diameter is about 20–30 nm, whereas in some cases, the depth equals the superconductor thickness. In Table 1 the percentage of Fe, As, and Ba obtained by EDX

TABLE 1: EDX analysis relative to the white cross markers reported in Figure 2(c).

Position	Fe (at%)	As (at%)	Ba (at%)
1	95.72	4.28	—
2	97.95	2.05	—
3	29.12	56.04	14.84
4	33.71	55.66	4.63
5	37.15	52.43	10.42
6	40.14	54.58	5.28
7	40.29	53.68	6.03

analysis is reported. It must be noted that even close to the superconductor surface a large percentage (30%–40%) of Fe is still detected, probably due to its oxidation or diffusion during the fabrication process.

For determining magnetic properties of the samples with and without the Fe buffer layer, MOKE measurements at both room temperature and 5 K have been carried out.

Figure 3(a) reports the Kerr rotation, θ_k, as a function of the applied external magnetic field. It can be noted that the Ba-122/Fe sample (red and black squares) is characterized by hysteresis loop at both 300 K and 5 K (the latter temperature corresponds to the superconducting phase), while the Ba-122 sample (open squares) does not present any magnetization at room temperature or at 5 K (data at 5 K are not shown). This conclusion was verified for field intensities up to 1 T. These results clearly reveal the ferromagnetic behaviour of the Fe buffer layer.

We also observed that the Ba-122/Fe sample presents smaller residual magnetization in the superconducting phase compared to the room temperature case, whereas the coercive fields remain quite the same (about 2.5 mT).

The smaller residual magnetization in the low temperature case can be explained as follows: Since the optical penetration depth into Ba-122 of radiation at $\lambda = 633$ nm wavelength is about 20–30 nm [24], it is reasonable to assume that the laser beam actually penetrates into the superconductor but is strongly absorbed before reaching the Fe buffer layer. On the other hand, taking into account the above-mentioned TEM analysis, we can argue that the laser beam focal spot (with a diameter of about 100 μm) probes an area where several holes are present. From Figure 2(b), we can estimate that the total linear dimension of holes amounts to approximately 10% of the whole section length, corresponding to about 20% of the surface area. Thus, as a result of AFM and TEM analyses, we deduce that the MOKE signals from our samples consist of two main contributions: The first arises from the fraction (>20%) of the laser beam cross section that directly hits the Fe buffer layer passing through the Ba-122 holes; such a contribution is expected to be temperature independent. The second is originated by the large Fe fraction (30–40%) detected close to the Ba-122 outer surface (within a laser beam penetration depth). As a consequence, the smaller residual magnetization observed at low temperature can be attributed to the Meissner effect occurring in the superconductor. This acts as a partial shield
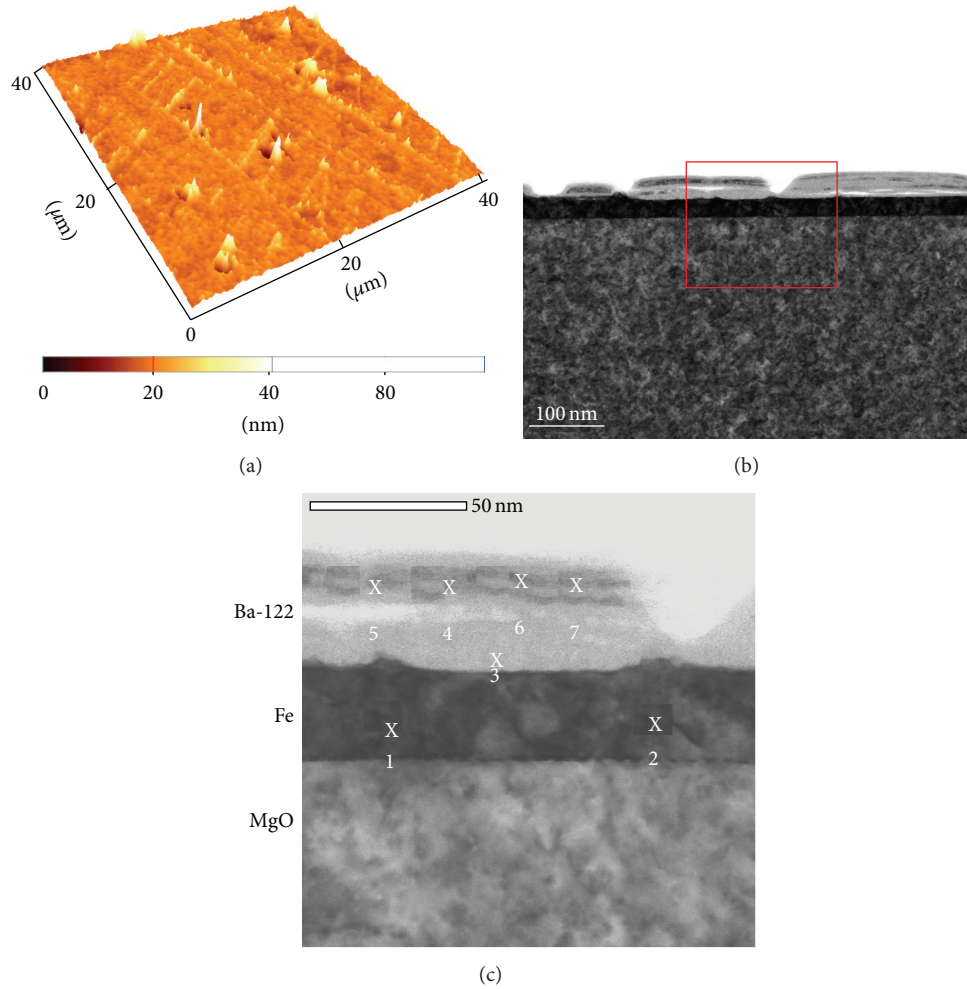
(a)

(b)

(c)

FIGURE 2: (a) AFM image (40×40 μm) of a Co-doped Ba-122 (100 nm)/Fe thin film and (b) TEM image of the same sample. The TEM image within the red square in (b) is enlarged in (c).

of the external magnetic field, which is, thus, unable to completely magnetize the fraction of Fe close to the sample outer surface.

In order to confirm this interpretation, MOI measurements have been performed at both low and room temperature. In MOI image at room temperature (Figure 3(b)), the magnetic field generated by the Fe buffer layer demonstrates its ferromagnetic nature and that the spontaneous magnetization lies in the film plane, in agreement with the MOKE hysteretic loop shown in Figure 3(a). On the other hand, the MOI pattern at low temperature (Figure 3(c)) shows the critical state of a disordered superconductor, with many laminar defects and grain boundaries, which are responsible for a disordered vortex distribution. However, the whole film is still superconducting, and a percolating zero-resistance state is even demonstrated by transport characterization [25]. Low contrast in the MOI image, corresponding to a weak critical current density, is unlikely due to the effect of the magnetic film which has in-plane anisotropy [26]. Therefore, from MOI analysis we can deduce that Ba-122 is not strongly affected by the underlying Fe magnetic film, but it rather presents a superconducting phase. However, in some regions

of the surface the Meissner effect takes place and partially screens the magnetization of the Fe buffer layer.

In order to confirm the minor role of the Fe buffer layer on superconducting properties of Ba-122 thin films, we carried out transient reflectivity experiments at both 300 K and 20 K on Ba-122 (100 nm)/CaF$_2$, Ba-122 (100 nm)/Fe (20 nm)/MgO, and Fe (50 nm)/MgO thin films, respectively (see Figure 4).

First, we can assume that reflection from the Ba-122/Fe sample is essentially due to the upper Ba-122 thin film, since its thickness exceeds the optical penetration depth of laser radiation (~26 nm [24]). Moreover, it is worth noting that the transient reflectivity of the Fe/MgO thin film presents completely different relaxation dynamics as compared to other films at both 300 K and 20 K, namely, in the normal and superconducting phases, respectively (Figures 4(a)-4(b)).

We further investigated the influence of Fe buffer layer on superconducting behaviour. Transient reflectivity measurements with temperatures ranging from 5 K to 230 K, both below and above samples superconducting transition ($T_c \cong$ 26 K), have been carried out. Transient reflectivity curves as a function of time following the excitation pulse are shown in Figures 4(a)-4(b). The experimental data have been
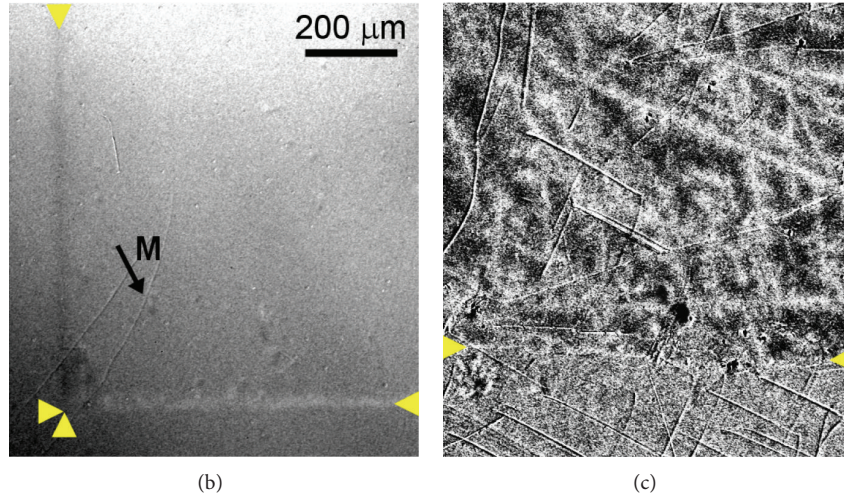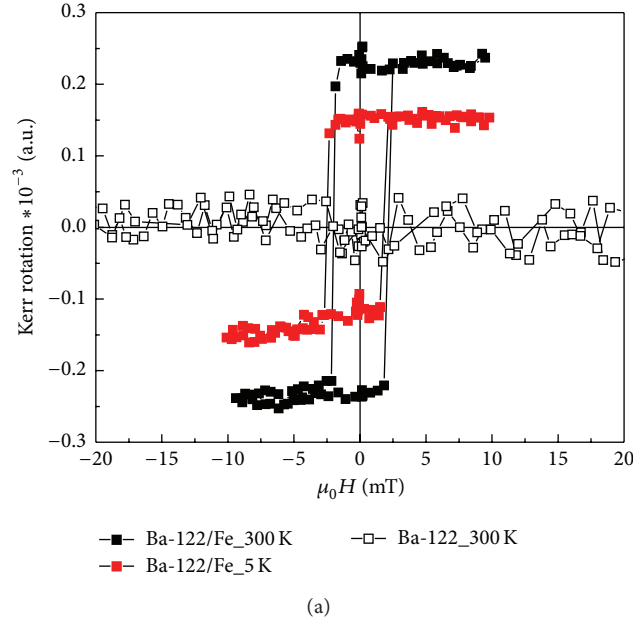
(a)

(b)

(c)

FIGURE 3: (a) Hysteresis loops obtained by means of MOKE measurements: Ba-122/Fe at 5 K (red squares) and 300 K (black squares); Ba-122 thin film at 300 K (open squares); (b) MOI on Ba-122/Fe film at room temperature. Since MOI is sensitive to out-of-plane magnetic fields, the in-plane magnetization direction can be inferred from the signal at the edges (indicated by yellow arrows). (c) MOI at low temperature ($T = 10$ K), after Zero-Field Cooling (ZFC) with applied magnetic field $H = 1.5$ mT; bright regions: preferential vortex penetration and normal zones; dark regions: screened zones.

fitted by a double exponential function in case of $T < T_c$, whereas a single exponential fitting function has been used for temperatures above T_c. The longest decay time, τ_{slow}, in the nanosecond time-scale (only present for $T < T_c$) is reported as a function of temperature in Figure 4(c). On the contrary, the short relaxation time, τ_{fast}, in the subpicosecond region, is observed throughout the entire range of temperatures. And its behaviour as a function of temperature is reported in the inset of Figure 4(c). However, since we are only interested in the superconducting phase, both relaxation times are showed for $T < T_c$.

From Figure 4(c) we noticed that in the superconducting state ($T < T_c$) both τ_{fast} and τ_{slow} rapidly increase as T approaches T_c. In particular, the variation of τ_{fast} close to T_c amounts to few tenths of femtosecond (inset of Figure 4(c)), whereas τ_{slow} varies as much as 2 ps. This divergence-like behavior near T_c typically occurs in the framework of quasi-particle (QP) recombination in a superconductor presenting a temperature dependent gap below T_c [27], when the bottle-neck regime takes place [12, 28]. The bottleneck effect consists in the creation of a large nonequilibrium phonon population, due to the emission of phonons by photoexcited electrons and holes, after absorption of a photon. In particular, phonons with energy exceeding the gap ($\hbar\omega_{ph} > 2\Delta$) can subsequently excite QPs from the condensate, but these recombine again and so a bottleneck occurs, in which high frequency phonons
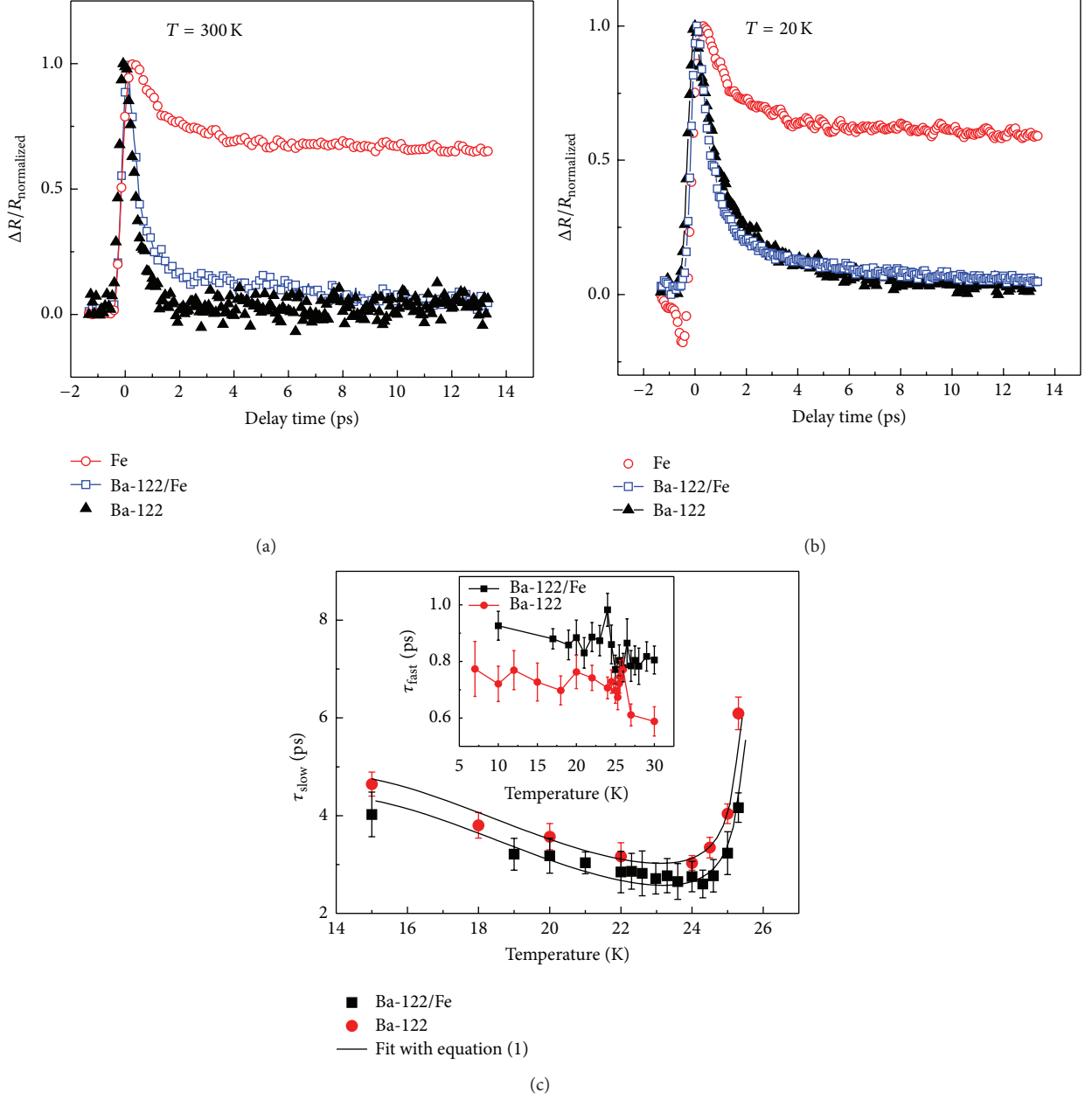
(a)

(b)

(c)

FIGURE 4: Normalized transient reflectivity of Ba-122/CaF$_2$, Ba-122/Fe/MgO, and Fe/MgO thin films at 300 K (a) and 20 K (b); (c) the τ_{slow} divergence-like behaviour for the two thin films. The solid lines represent the best fit of (1); inset: τ_{fast} versus temperature for the same two films.

are temporarily in quasi-equilibrium with QPs [29]. In such a framework, the QP recombination time can be expressed as [27]

$$\tau = -\frac{\hbar \omega_{\text{ph}}^2}{12\Gamma_\omega \Delta(T)^2} \ln\left(\frac{E}{2N(0)\Delta_0^2} + e^{-\Delta(T)/k_B T}\right), \quad (1)$$

where E is the laser pulse energy, ω_{ph} the typical phonon frequency, $N(0)$ the density of states (DOS), Γ_ω a characteristic phonon linewidth, and $\Delta(T)$ the superconducting gap with the BCS temperature dependence [27]. Thus, we fitted the experimental points of Figure 4(c) with (1) using Δ_0 and

$\hbar \omega_{\text{ph}}^2 / 12\Gamma_{\omega_{\text{ph}}}$ as fitting parameters. The solid black lines in Figure 4(c) are the results of the best fit for the two films Ba-122/Fe and Ba-122. It is worth noting the divergence predicted by (1) as the temperature approaches T_c.

The best fitting values of the superconducting gap are $\Delta_0 = (3.17 \pm 0.03)$ meV and $\Delta_0 = (2.72 \pm 0.02)$ meV for Ba-122/Fe and Ba-122 films, respectively, in agreement with the superconducting gap value estimated with different techniques [14, 30, 31]. Such an agreement also confirms our interpretation that in Ba-122 samples the relaxation channel associated with τ_{slow} is described by the creation of high frequency phonon (bosons) with $\omega_{\text{ph}} > 2\Delta$. These phonons,

in turn, break additional Cooper pairs and, hence, inhibit QP recombination. On the other hand, the superconducting gap Δ_0 estimated for Ba-122/Fe is larger compared to the sample without the Fe buffer layer, which implies that the Fe buffer layer affects the Fermi surface without destroying superconductivity. It is worth mentioning that a complete transient reflectivity data analysis concerning the Ba-122/Fe superconducting samples evidenced the presence of two gaps, as reported elsewhere [15].

4. Conclusions

In this work the analysis of Co-doped Ba-122 with and without Fe buffer layer is reported. AFM and TEM measurements demonstrate an irregular surface morphology in the Ba-122 thin film in presence of Fe buffer layer. MOKE analysis shows the ferromagnetic nature of the sample (from room temperature down to 5 K) due to the presence of Fe, confirmed by the independence of coercive field from temperature. On the contrary, the Ba-122 thin film without Fe buffer layer does not present any hysteresis loop (up to 1 T). This result is confirmed by MOI characterization that showed the coexistence of ferromagnetism of the Fe buffer layer with superconductivity of the Ba-122 film. The pump-probe spectroscopy confirms that the Fe buffer layer does not alter the superconducting properties of the Ba-122 thin film. In particular, the superconducting gap of Ba-122/Fe resulted in being slightly larger than the Ba-122 layer. In conclusion, the presence of the Fe buffer layer does not modify the superconducting properties under our deposition condition while allowing a bilayer with both superconducting and ferromagnetic properties. This result could be noteworthy in the field of electronic applications.

Conflict of Interests

The authors declare that there is no conflict of interests regarding the publication of this paper.

Acknowledgment

References

[1] T. Katase, Y. Ishimaru, A. Tsukamoto et al., "DC superconducting quantum interference devices fabricated using bicrystal grain boundary junctions in Co-doped BaFe$_2$As$_2$ epitaxial films," *Superconductor Science and Technology*, vol. 23, no. 8, Article ID 082001, 2010.

[2] S. Lee, J. Jiang, Y. Zhang et al., "Template engineering of Co-doped BaFe$_2$As$_2$ single-crystal thin films," *Nature Materials*, vol. 9, no. 5, pp. 397–402, 2010.

[3] T. Katase, H. Hiramatsu, T. Kamiya, and H. Hosono, "High critical current density 4 MA/cm^2 in Co-doped BaFe$_2$As$_2$ epitaxial films grown on (La,Sr)(Al,Ta)O$_3$ substrates without buffer layers," *Applied Physics Express*, vol. 3, no. 6, Article ID 063101, 2010.

[4] K. Iida, J. Hänisch, R. Hühne et al., "Strong T_c dependence for strained epitaxial Ba(Fe$_{1-x}$Co$_x$)$_2$As$_2$ thin films," *Applied Physics Letters*, vol. 95, Article ID 192501, 2009.

[5] F. Kurth, K. Iida, S. Trommler et al., "Electronic phase diagram of disordered Co doped BaFe$_2$As$_{2-\delta}$," *Superconductor Science and Technology*, vol. 26, no. 2, Article ID 025014, 2013.

[6] F. Kurth, E. Reich, J. Hänisch et al., "Versatile fluoride substrates for Fe-based superconducting thin films," *Applied Physics Letters*, vol. 102, no. 14, Article ID 142601, 2013.

[7] T. Thersleff, K. Iida, S. Haindl et al., "Coherent interfacial bonding on the FeAs tetrahedron in Fe/Ba(Fe$_{1-x}$Co$_x$)$_2$As$_2$ bilayers," *Applied Physics Letters*, vol. 97, Article ID 022506, 2010.

[8] T. Mertelj, V. V. Kabanov, C. Gadermaier et al., "Distinct pseudogap and quasiparticle relaxation dynamics in the superconducting state of nearly optimally doped SmFeAsO$_{0.8}$F$_{0.2}$ single crystals," *Physical Review Letters*, vol. 102, no. 11, Article ID 117002, 2009.

[9] D. H. Torchinsky, J. W. McIver, D. Hsieh et al., "Nonequilibrium quasiparticle relaxation dynamics in single crystals of hole- and electron-doped BaFe$_2$As$_2$," *Physical Review B*, vol. 84, no. 10, Article ID 104518, 2011.

[10] T. Mertelj, L. Stojchevska, N. D. Zhigadlo, J. Karpinski, and D. Mihailovic, "Normal state bottleneck and nematic fluctuations from femtosecond quasiparticle relaxation dynamics in Sm(Fe,Co)AsO," *Physical Review B: Condensed Matter and Materials Physics*, vol. 87, no. 17, Article ID 174525, 2013.

[11] P. Kusar, J. Demsar, D. Mihailovic, and S. Sugai, "A systematic study of femtosecond quasiparticle relaxation processes in La$_{2-x}$Sr$_x$CuO$_4$," *Physical Review B: Condensed Matter and Materials Physics*, vol. 72, no. 1, Article ID 014544, 2005.

[12] V. V. Kabanov, J. Demsar, and D. Mihailovic, "Kinetics of a superconductor excited with a femtosecond optical pulse," *Physical Review Letters*, vol. 95, no. 14, Article ID 147002, 2005.

[13] E. E. M. Chia, D. Talbayev, J.-X. Zhu et al., "Ultrafast pump-probe study of phase separation and competing orders in the underdoped (Ba,K)Fe$_2$As$_2$ superconductor," *Physical Review Letters*, vol. 104, no. 2, Article ID 027003, 2010.

[14] D. H. Torchinsky, G. F. Chen, J. L. Luo, N. L. Wang, and N. Gedik, "Band-dependent quasiparticle dynamics in single crystals of the Ba$_{0.6}$K$_{0.4}$Fe$_2$As$_2$ superconductor revealed by pump-probe spectroscopy," *Physical Review Letters*, vol. 105, no. 2, Article ID 027005, pp. 027005–027008, 2010.

[15] C. Bonavolontà, C. de Lisio, M. Valentino et al., "Evaluation of superconducting gaps in optimally doped Ba(Fe$_{1-x}$Co$_x$)$_2$As$_2$/Fe bilayers by ultrafast time-resolved spectroscopy," *Physica C: Superconductivity*, vol. 503, pp. 132–135, 2014.

[16] S. Visnovsky, *Optics in Magnetic Multilayers and Nanostructures*, CRC Press, Taylor & Francis Group, 2006.

[17] M. Tamisari, G. Ausanio, V. Guidi et al., "Magnetic and structural investigation of growth induced magnetic anisotropies in Fe$_{50}$Co$_{50}$ thin films," *EPJ Web of Conferences*, vol. 40, Article ID 09002, 4 pages, 2012.

[18] Q. Y. Lei, M. Golalikhani, D. Y. Yang et al., "Structural and transport properties of epitaxial Ba(Fe$_{1-x}$Co$_x$)$_2$As$_2$ thin films on various substrates," *Superconductor Science and Technology*, vol. 27, no. 11, Article ID 115010, 2014.

[19] E. Kita, M. Ochi, T. Erata, and A. Tasaki, "Magnetic properties of Fe/fluorides (CaF$_2$, LiF) multilayered thin films," *Journal of Magnetism and Magnetic Materials*, vol. 117, no. 1-2, pp. 294–300, 1992.

[20] F. Laviano, D. Botta, A. Chiodoni et al., "An improved method for quantitative magneto-optical analysis of superconductors," *Superconductor Science and Technology*, vol. 16, no. 1, pp. 71–79, 2003.

[21] G. P. Pepe, L. Parlato, N. Marrocco et al., "Novel superconducting proximized heterostructures for ultrafast photodetection," *Cryogenics*, vol. 49, no. 11, pp. 660–664, 2009.

[22] T. Plecenik, M. Gregor, R. Sobota et al., "Surface transport properties of Fe-based superconductors: the influence of degradation and inhomogeneity," *Applied Physics Letters*, vol. 103, no. 5, Article ID 052601, 2013.

[23] D. Daghero, P. Pecchio, F. Laviano et al., "Advanced surface characterization of $Ba(Fe_{0.92}Co_{0.08})_2As_2$ epitaxial thin films," *Applied Surface Science*, vol. 312, pp. 23–29, 2014.

[24] S. Kumar, L. Harnagea, S. Wurmehl, B. Buchner, and A. K. Sood, "Acoustic and optical phonon dynamics from femtosecond time-resolved optical spectroscopy of the superconducting iron pnictide $Ca(Fe_{0.944}Co_{0.056})_2As_2$," *EPL*, vol. 100, no. 5, Article ID 57007, 2012.

[25] K. Iida, S. Haindl, T. Thersleff et al., "Influence of Fe buffer thickness on the crystalline quality and the transport properties of $Fe/Ba(Fe_{1-x}Co_x)_2As_2$ bilayer," *Applied Physics Letters*, vol. 97, Article ID 172507, 2010.

[26] F. Laviano, L. Gozzelino, R. Gerbaldo et al., "Interaction between vortices and ferromagnetic microstructures in twinned cuprate/manganite bilayers," *Physical Review B*, vol. 76, no. 21, Article ID 214501, 2007.

[27] V. V. Kabanov, J. Demsar, B. Podobnik, and D. Mihailovic, "Quasiparticle relaxation dynamics in superconductors with different gap structures: theory and experiments on $YBa_2Cu_3O_{7-\delta}$," *Physical Review B*, vol. 59, no. 2, pp. 1497–1506, 1999.

[28] J. Demsar, J. L. Sarrao, and A. J. Taylor, "Dynamics of photoexcited quasiparticles in heavy electron compounds," *Journal of Physics Condensed Matter*, vol. 18, no. 16, pp. R281–R314, 2006.

[29] Y. Gong, W. Lai, T. Nosach et al., "Distinct quasiparticle relaxation dynamics in an electron-doped superconductor, $BaFe_{1.9}Ni_{0.1}As_2$," *New Journal of Physics*, vol. 12, Article ID 123003, 2010.

[30] B. Mansart, D. Boschetto, A. Savoia et al., "Ultrafast transient response and electron-phonon coupling in the iron-pnictide superconductor $Ba(Fe_{1-x}Co_x)_2As_2$," *Physical Review B*, vol. 82, no. 2, Article ID 024513, 2010.

[31] L. Stojchevska, T. Mertelj, J.-H. Chu, I. R. Fisher, and D. Mihailovic, "Doping dependence of femtosecond quasiparticle relaxation dynamics in $Ba(Fe,Co)_2As_2$ single crystals: evidence for normal-state nematic fluctuations," *Physical Review B: Condensed Matter and Materials Physics*, vol. 86, no. 2, Article ID 024519, 2012.

Journal of
Gravity

Journal of
Photonics

**The Scientific
World Journal**

Journal of
Soft Matter

Advances in
Condensed Matter Physics

Journal of
Fluids

Journal of
Aerodynamics

International Journal of
Statistical Mechanics

Hindawi

Submit your manuscripts at
http://www.hindawi.com

International Journal of
Optics

Journal of
**Computational
Methods in Physics**

Advances in
High Energy Physics

Journal of
Thermodynamics

Physics
Research International

Advances in
Astronomy

Journal of
Solid State Physics

Journal of
Astrophysics

International Journal of
Superconductivity

Journal of
Biophysics

Journal of
Atomic and
Molecular Physics